Surgical Endoscopy (2024) 38:6938–6947
https://doi.org/10.1007/s00464-024-11295-8

DYNAMIC MANUSCRIPT

Use of indocyanine green-human serum albumin complexes in fluorescence image-guided laparoscopic anatomical liver resection: a case series study (with video)

Fengwei Gao[1] · Qingyun Xie[1] · Xiaoyun Ran[2] · Xin Zhao[3] · Manyu Yang[3] · Kangyi Jiang[3] · Tianyang Mao[3] · Jiayin Yang[1] · Kun Li[2] · Hong Wu[1]

Received: 3 July 2024 / Accepted: 13 September 2024 / Published online: 29 September 2024

Abstract

Background This study aimed to investigate the feasibility and efficacy of near-infrared fluorescence-guided laparoscopic anatomical hepatectomy (LAH) using a novel indocyanine green (ICG)-human serum albumin complex (HSA) in patients with hepatocellular carcinoma.

Methods Clinical data of hepatocellular carcinoma patients who underwent ICG-HSA fluorescence-guided LAH at our center from January 2024 to April 2024 were prospectively collected and analyzed. Ultraviolet absorption spectroscopy was used to test the absorption and stability of ICG-HSA complex solutions under different conditions. After determining the optimal ratio, the complex was administered intravenously during surgery to perform negative staining via Glissonean pedicle isolation. LAH was performed along the fluorescence-demarcated boundaries.

Results Thirty-one patients were included (24 men; mean age, 54.61 ± 13.54 years). The median maximum tumor diameter was 2.80 (interquartile range [IQR], 2.00–4.00) cm. S8 segmentectomy (22.6%) and right posterior segmentectomy (19.4%) were the most common resections performed. Successful fluorescence negative staining was achieved in all patients using ICG and HSA at a 1:6 molar ratio at room temperature. Mean operation time was 297.58 ± 85.53 min, Median intraoperative blood loss was 100.0 mL (IQR, 50.0–200.0). The median surgical margin distance was 0.90 cm (IQR, 0.40–1.50). The postoperative complication rate was 45.2% (35.5% Clavien–Dindo grade I and 9.7% grade II). The median length of hospital stay was 5.0 days (IQR, 4.0–5.0).

Conclusion ICG-HSA-assisted LAH is safe and feasible. Compared with free ICG, the novel ICG-HSA complex exhibits better optical properties and in vivo stability, which can improve the accuracy of intraoperative liver segment localization and optimize the anatomical dissection plane. It has the potential to become an ideal fluorescent imaging agent for anatomical hepatectomy.

Keywords ICG-HSA complex · Near-infrared fluorescence · Laparoscopic anatomical hepatectomy · Hepatocellular carcinoma

Hepatocellular carcinoma is the sixth most common malignancy and the fourth leading cause of cancer-related

Fengwei Gao, Qingyun Xie and Xin Zhao these authors contributed equally to this work.

✉ Hong Wu
wuhong@scu.edu.cn

Kun Li
Kli@scu.edu.cn

[1] Liver Transplantation Center, State Key Laboratory of Biotherapy and Cancer Center, West China Hospital, Sichuan University and Collaborative Innovation Center of Biotherapy, 37 Guoxue Lane, Wuhou District, Chengdu 610041, Sichuan, China

[2] Key Laboratory of Green Chemistry and Technology of Ministry of Education, College of Chemistry, Sichuan University, Chengdu 61064, Sichuan, China

[3] Department of Hepato-Pancreato-Biliary Surgery, People's Hospital of Leshan, Leshan 614000, China

mortality worldwide [1]. Liver resection remains the primary curative treatment option. Compared with non-anatomical liver resection, laparoscopic anatomical hepatectomy enables a more thorough removal of the liver segment or subsegment harboring the tumor and eliminates potential intrahepatic metastases, thus improving oncological outcomes. As a result, it is highly advocated by liver surgeons [2, 3]. However, accurately determining the borders of liver segments and subsegments and designing the optimal resection plane during surgery remains challenging, especially in minimally invasive liver resection procedures such as laparoscopic hepatectomy.

In recent years, indocyanine green (ICG) dye-mediated near-infrared fluorescence (NIF) imaging has shown promise in assisting anatomical liver resection. It enables accurate localization of the targeted liver segment, helps to reduce postoperative dysfunction of the remnant liver, and improves oncological outcomes [4, 5]. After intravenous injection, ICG rapidly binds to plasma proteins and is taken up by hepatocytes, allowing real-time visualization of liver tumors and parenchyma. However, it is poorly soluble in water, susceptible to concentration-dependent aggregation, and has a short hepatic retention time. These characteristics limit its widespread application to some extent [6, 7].

To overcome these limitations, we have developed a novel complex combining human serum albumin (HSA) and ICG (ICG-HSA). HSA is an endogenous protein which can improve the dispersibility and fluorescence performance of ICG in aqueous solution [8, 9]. HSA can bind to ICG to form nanoparticles approximately 4–7 nm in size, which reduces the number of free ICG monomers and avoids background interference caused by their free diffusion [10]. Compared with free ICG, ICG-HSA exhibits better stability and longer hepatic retention time. We hypothesized that ICG-HSA might be an ideal NIF fluorescent tracer for guiding laparoscopic anatomical hepatectomy. Therefore, we conducted a preliminary prospective clinical study to evaluate the feasibility and effectiveness of NIF-guided laparoscopic anatomical hepatectomy using ICG-HSA in patients with hepatocellular carcinoma. The study was registered on ClinicalTrials.gov and conducted in compliance with the Declaration of Helsinki and all relevant guidelines and regulations for research involving human subjects, human material, or human data.

Methods

This study has been reported in line with the PROCESS criteria [11].

Patient inclusion and exclusion criteria

Inclusion criteria: (1) Patients aged 18–75 years with malignant liver tumors requiring laparoscopic anatomical hepatectomy; (2) Preoperative Child–Pugh class A or B; (3) No contraindication to laparoscopic liver resection; (4) Expected survival ≥ 3 months; (5) Eastern Cooperative Oncology Group performance status score 0 or 1; and (6) Laboratory testing within 7 days prior to enrollment meeting the following conditions: white blood cell count $\geq 2.5 \times 10^9$/L, absolute neutrophil count $\geq 1.5 \times 10^9$/L, platelet count $\geq 75 \times 10^9$/L, hemoglobin ≥ 90 g/L; international normalized ratio ≤ 1.5 × upper limit of normal (ULN); serum creatinine ≤ 1.5 × ULN; total bilirubin ≤ 1.5 × ULN.

Exclusion criteria: (1) No obvious ischemic demarcation line after intraoperative blocking or isolation of the target liver pedicle, or liver fluorescence reaching an intensity that interferes with the operation before intraoperative intravenous injection of ICG; (2) ICG retention rate at 15 min ≥ 20%; (3) Severe cardiopulmonary disease precluding surgery under general anesthesia; (4) Clinically significant ascites or pleural effusion; (5) Active bleeding or coagulation dysfunction; (6) Hepatic encephalopathy; (7) Allergy to ICG; (8) History of gastrointestinal bleeding within the past 6 months or tendency for gastrointestinal bleeding; (9) Severe gastroesophageal varices requiring treatment; (10) Objective evidence of past or present severely impaired lung function; and (11) Any clinical or laboratory abnormalities that may affect the safety evaluation.

Preparation and testing of the ICG-HSA complex

Commercially available ICG and HSA solutions were mixed at different ratios at room temperature to ensure thorough mixing of ICG and protein and then formulated into test solutions of varying concentrations. Subsequently, an ultraviolet spectrophotometer was used to measure changes in the absorption spectra of the complex solutions at different mixing times and ratios. After determining the optimal ratio and time, the stability at different temperatures was tested using the same method. The complex was then applied for use after the binding ability of ICG and HSA was verified via in vitro experiments and the key components and ratios of the novel ICG-HSA complex determined.

Surgical procedure

Based on preoperative three-dimensional reconstruction images, an anatomical plan was formulated to resect the liver segment or lobe where the tumor was located. All laparoscopic anatomical hepatectomies were performed

by the same hepatobiliary surgical team. Each surgeon had over 10 years of experience and had completed more than 100 laparoscopic hepatectomies. After induction of general endotracheal anesthesia, patients were placed in the supine position for laparoscopic hepatectomy. The intra-abdominal pressure was set at 10–14 mm Hg. Central venous pressure was monitored and maintained below 5 cm H_2O. A Harmonic ultrasonic scalpel (Ethicon, Cincinnati, OH, USA) was used to adequately mobilize the hepatic ligaments. The guideline-recommended "negative-staining method" was used to complete the hepatectomy [5].The hepatic pedicle of the lobe or segment planned for resection was isolated and occluded using the Glissonean pedicle transection technique after confirming the diseased area. Then, the ICG-HSA complex was administered intravenously using an infusion pump at a rate of 1 mL per minute. Liver fluorescence imaging was performed in fluorescence mode using the FloNavi 214 K NIF system (OptoMedic, Guangzhou, China). Gain value was set to 2 and the injection of ICG-HSA was stopped when the liver surface began to show fluorescence imaging. Intraoperative ultrasonography was used to confirm whether the tumor was located in the imaged liver segment. After confirming that the tumor was located in the non-fluorescent area and the resection margin was sufficient, the liver segment was resected along the fluorescent boundary while the hepatoduodenal ligament was clamped (Pringle maneuver) to stop liver blood flow. After the liver resection was completed, the liver specimen was extracted through the umbilical incision. Then, the pneumoperitoneum was deflated, the puncture sites were sutured, and the operation was completed (as shown in Fig. 1 and Video 1).

Perioperative data collection

Data collected included patient demographics (gender, age, body mass index), preoperative laboratory test results (coagulation function, platelet count, liver function, tumor marker levels), tumor characteristics (maximum diameter, hepatitis B virus infection status), and surgery characteristics (type of liver resection, operation time, intraoperative blood loss, presence of satellite nodules, microvascular invasion, tumor differentiation grade, and surgical margin distance). Postoperative follow-up outcomes included complications (Clavien–Dindo classification [12]), length of hospital stay, and liver function recovery on postoperative days 1, 2, and 3 (as measured by levels of alanine and aspartate transaminases, albumin, and total bilirubin).

Statistical analysis

Data analysis was performed using SPSS software version 23.0 (IBM Corp., Armonk, NY, USA). Categorical variables are expressed as frequencies with percentage. Continuous variables with a normal and non-normal distribution are presented as means with standard deviation and medians with interquartile range (IQR), respectively.

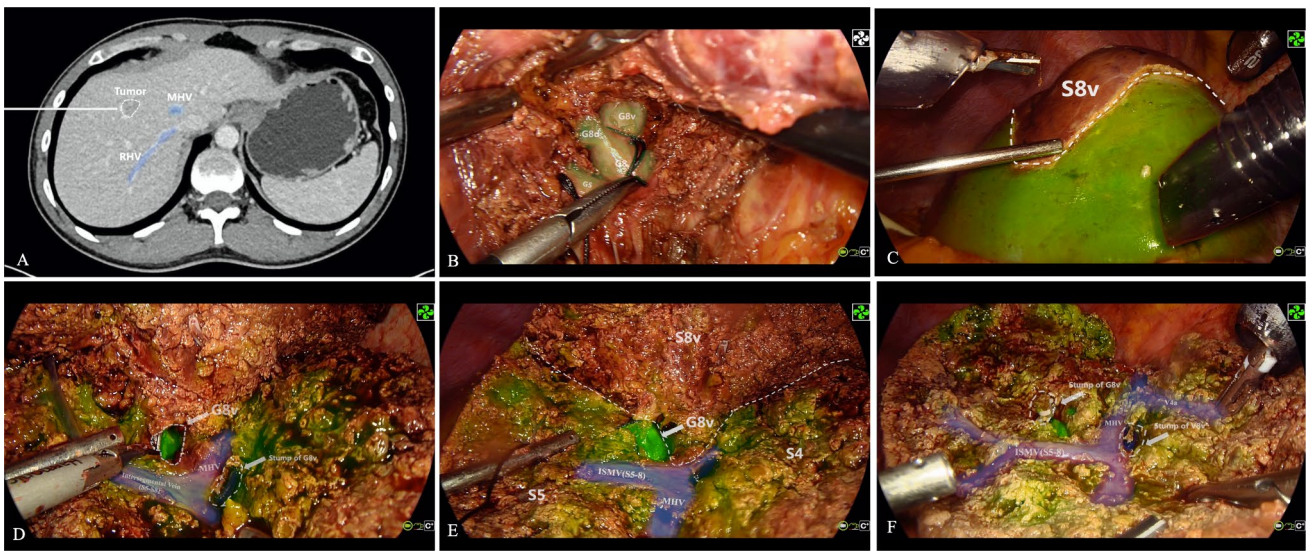

Fig. 1 The novel ICG and HSA complex combined with " negative-staining" fluorescence-guided laparoscopic anatomical sub-segmentectomy. **A** Preoperative enhanced computed tomography revealed that the tumor was situated in the ventral segment of segment 8 (S8v). **B** The ventral branch of segment VIII (G8v) was identified and occluded. **C** After successful negative staining, the fluorescent demarcation line between S8v and the parenchyma intended for preservation was highly distinct and conspicuous. **D**-**E** After the complete separation of S8v from segments 5 and 4A, the root of G8v was visibly exposed in the surgical field. **F** Only two ligation clips, which were used to ligate G8v and the vein draining S8v were visible in the surgical area. Additionally, the vein draining segment 4A, the middle hepatic vein, and the intersegmental vein were all clearly exposed in this cross-section

Results

Patient characteristics

The study included 31 patients who underwent ICG-HSA fluorescence-guided laparoscopic liver resection at our center from January 2024 to April 2024. Twenty-four patients were male (77.4%). Mean age was 54.61 ± 13.54 years and mean body mass index was 23.59 ± 2.81 kg/m^2. Preoperative prothrombin time international normalized ratio, platelet count, liver function, and tumor marker levels (alpha fetoprotein, protein induced by vitamin K absence or antagonist-2) were all within normal range. The median maximum tumor diameter was 2.80 cm (IQR, 2.00–4.00) and 27 patients (87.1%) had concomitant hepatitis B virus infection (Table 1).

Table 1 Patient characteristics

Variables	$n = 31$
Sex, male, n (%)	24(77.4%)
Age, mean ± SD, y	54.61 ± 13.54
BMI, mean ± SD, kg/m^2	23.59 ± 2.81
PT, median (IQR), s	10.90 (10.45–11.75)
INR, median (IQR)	0.99 (0.95–1.05)
PLT, mean ± SD,10*^{9}/L	154.61 ± 49.84
ALT, median (IQR),U/L	26.00 (16.00–35.50)
AST, median (IQR),U/L	25.00 (18.00–32.00)
Albumin, mean ± SD, g/L	43.42 ± 3.14
TB, mean ± SD, μmol/L	13.42 ± 5.13
AFP, median (IQR), ng/ml	3.88 (2.77–65.59)
PIVKA-2, median (IQR), mAU/mL	54.00 (22.45–181.00)
Maximum diameter, median (IQR), cm	2.80 (2.00–4.00)
HBV(+), n (%)	27(87.1%)

IQR, interquartile range, *SD* Standard deviation, *BMI* Body Mass Index, *PT* Prothrombin Time, *INR* International Normalized Ratio, *PLT* Platelet, *ALT*, alanine transaminase, *AST* aspartate transaminase, *ALB* Albumin, *TB* Total Bilirubin AF

Optical properties, in vitro stability, and clinical formulation of the ICG-HSA complex

To determine the optimal binding time, optimal binding ratio, and stability of ICG-HSA, we tested the absorbance of ICG and HSA at different molar ratios at 0 h, 24 h, and 48 h. The experimental results showed that as the proportion of HSA increased, the stability of ICG-HSA improved. When the molar ratio of HSA to ICG was greater than 6, the stability of ICG-HSA was optimal and hardly changed with further increases in the ratio, as shown in Fig. 2A-D. On the basis of this, we investigated the stability of ICG-HSA at different temperatures. As shown in Fig. 2E-H, the stability of ICG-HSA increased with increasing temperature within the range of 0 °C–37 °C. However, at 50 °C, the stability decreased significantly, although it was still greatly improved compared with that of pure ICG molecules at room temperature. Overall, the ICG-HSA we prepared exhibited good stability under physiological conditions,

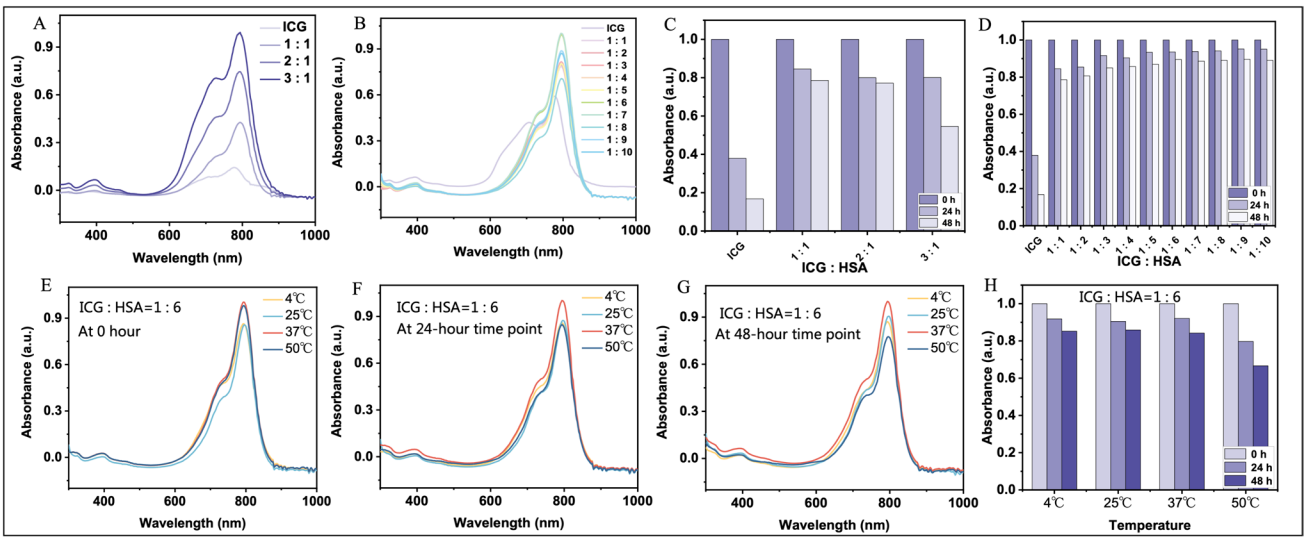

Fig. 2 Absorbance and stability test results of the ICG-HSA complex. **A-B** Absorbance tests: When ICG is in excess, the higher the proportion of ICG, the greater the absorbance; when HSA is in excess, the absorbance is highest at ICG:HSA = 1:6. **C-D** Stability tests: By comparing the changes in the absorbance of ICG and HSA at different molar ratios at 0 h, 24 h, and 48 h, we found that when ICG:HSA ≥ 1:6, the stability of ICG-HSA is optimal and hardly changes. **E–G** When ICG:HSA = 1:6 (molar ratio), from the time of solution preparation to 48 h after placement, the absorbance of the ICG-HSA complex is highest at 37 °C. **H** At 4 °C, 25 °C, and 37 °C, the ICG-HSA complex is relatively stable, while at 50 °C, the stability decreases

providing a solid material foundation for subsequent clinical applications.

Based on the results of the in vitro validation, we ultimately designed the clinical formulation of the ICG-HSA complex to be injected into the human body using commercially available human serum albumin (10 g/50 mL) and ICG (25 mg/10 mL). The clinical formulation is as follows: (1) It is known that the molar mass of HSA is approximately 66,500 g/mol [13] and the molar mass of ICG is 774.96 g/mol[6]. (2) According to the molar ratio of ICG:HSA = 1:6, through calculation, the required volume of the commercial HSA injection is approximately 0.02 mL, and the required volume of the commercial ICG is approximately 0.031 mL. (3) For the convenience of clinical use and to maintain the molar ratio, we mixed 2 mL of HSA and 0.3 mL of ICG and then added 15 mL of normal saline for dilution. Finally, a 20-mL syringe was used to hold the prepared complex solution. The syringe was connected to an intravenous infusion pump for uniform injection.

Perioperative outcomes

S8 segmentectomy (22.6%) and right posterior segmentectomy (19.4%) were the most common resections performed. The median surgical margin distance was 0.90 cm (IQR, 0.40–1.50). Satellite nodules were present in three patients (9.7%) and microvascular invasion in four (12.9%). Tumor differentiation was moderate in most patients (21 patients, 67.7%). Mean operation time was 297.58 ± 85.53 min. Median intraoperative blood loss was 100.0 mL (IQR, 50.0–200.0) mL. Grade 1 complications occurred in 11 patients (35.5%) and grade 2 in three (9.7%). Median hospital stay was 5.0 days (IQR, 4.0–5.0). After surgery, alanine and aspartate transaminase levels initially increased and then decreased, while albumin and total bilirubin levels remained relatively stable (Table 2).

Table 2 Surgical characteristics

Variables	$n = 31$
Hepatectomy type, n (%)	
LH(S2)	1(3.2%)
LH(S3)	1(3.2%)
LLLS	1(3.2%)
LLH	4(12.9%)
LH(S8)	7(22.6%)
LMS	2(6.5%)
LH(S5)	3 (9.7%)
LH(S6)	4(12.9%)
LH(S5 + S6)	2(6.5%)
LRPS	6(19.4%)
Surgical Margin, median (IQR),cm	0.90(0.40–1.50)
Satellite Nodule(+), n (%)	3 (9.7%)
MVI(+), n (%)	4(12.9%)
Differentiation, n (%)	
Poor	44(12.9%)
Moderate	21(67.7%)
Moderate–poor	6(19.4%)
Duration of surgery, mean ± SD, min	297.58 ± 85.53
Intraoperative bleeding, median (IQR), ml	100.0(50.0–200.0)
Postoperative complications, n (%)	
Grade I	11(35.5%)
Grade II	3 (9.7%)
Postoperative hospital stay, median (IQR), day	5.0(4.0–5.0)
POD1 ALT, median (IQR),U/L	394.0(317.5–525.5)
POD2 ALT, median (IQR),U/L	398.0(265.5–528.5)
POD3 ALT, median (IQR),U/L	257.0(191.0–349.0)
POD1 AST, median (IQR),U/L	420.0(263.5–565.5)
POD2 AST, median (IQR),U/L	235.0(184.5–391.0)
POD3 AST, median (IQR),U/L	102.0(71.5–176.5)
POD1 ALB, mean ± SD, g/L	34.39 ± 2.73
POD2 ALB, median (IQR), g/L	35.2(33.0–36.8)
POD3 ALB, mean ± SD, g/L	35.85 ± 3.83
POD1 TB, mean ± SD, μmol/L	23.37 ± 9.50
POD2 TB, median (IQR), μmol/L	22.70(19.15–30.90)
POD3 TB, median (IQR), μmol/L	21.40(17.95–28.95)

MVI Microvascular Invasion, *LH* laparoscopic hepatectomy, *LLH* laparoscopic left hemihepatectomy, *LLLS* laparoscopic left lateral sectionectomy, *LMS* laparoscopic monosegmentectomy, *LRH* laparoscopic right hemihepatectomy, *LRPS* laparoscopic right posterior sectionectomy, *POD* Postoperative Day

Surgical case demonstration

Stepwise fluorescence negative-staining technique

Stepwise resection of S5 and S6 was performed in two patients using the fluorescence negative-staining method as described in Fig. 3 and Video 2.

Fluorescence effects in other anatomical liver resections

Six patients underwent right posterior segmentectomy, one underwent segment 3 resection, and another underwent segment 2 resection. These are described in Fig. 4 as indicated as well as the Supplementary Material.

Discussion

According to current guidelines, fluorescence navigation technology is widely recognized as the most precise surgical approach to anatomical liver resection [5, 14, 15]. Compared with traditional white light laparoscopic liver resection, precise liver resection using ICG fluorescence navigation ensures safer surgical margins and improves the rate of R0

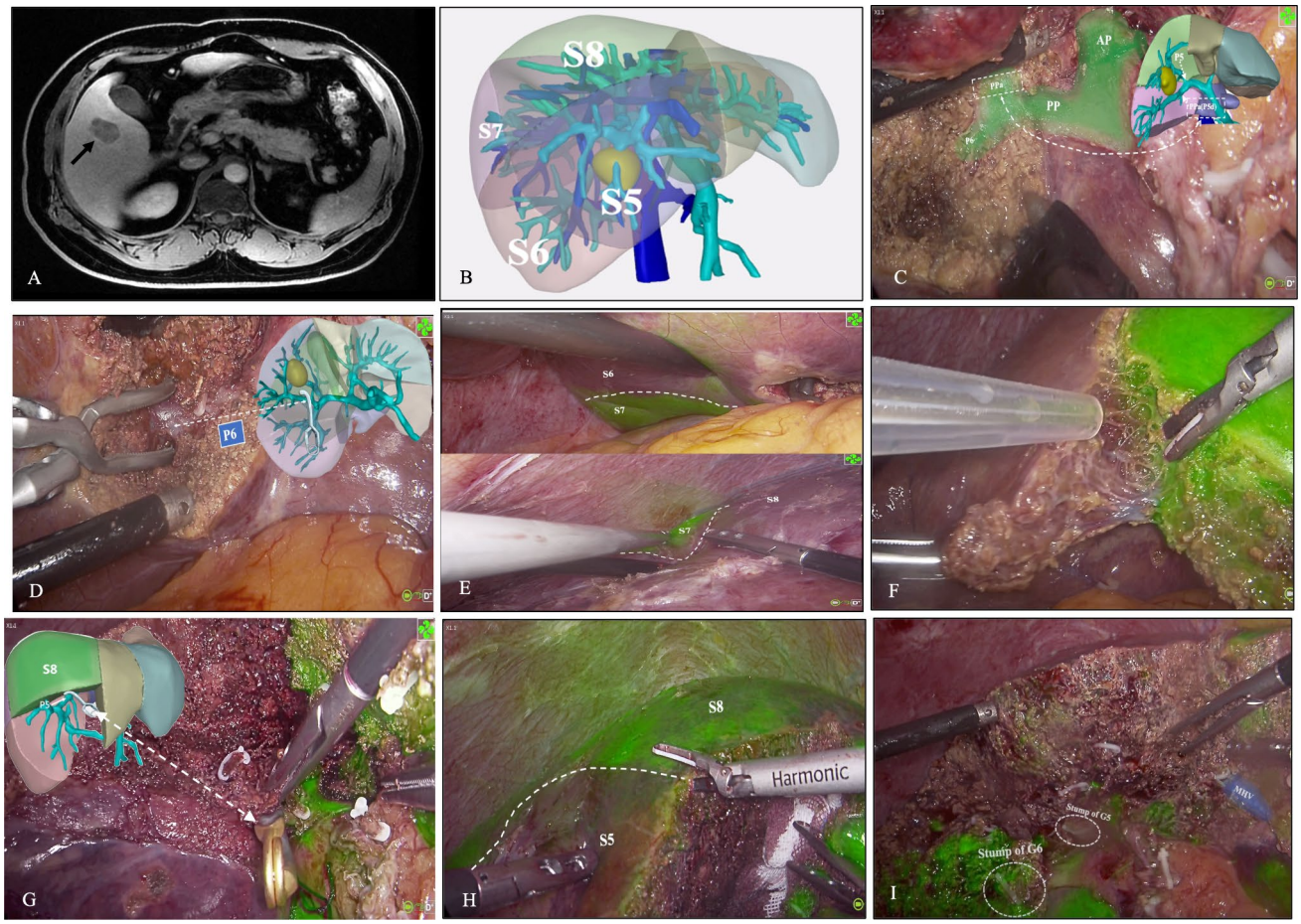

Fig. 3 **A** A 44-year-old man with hepatitis B virus-related cirrhosis presented with a hypervascular nodule at the junction of hepatic segments 5 and 6 (black arrow) on magnetic resonance imaging which was highly suspicious for hepatocellular carcinoma. **B** A three-dimensional reconstruction showed the tumor was closely attached to branches G5 and G6 and was located between hepatic veins V5 and V6. **C** The pedicle of segment 6 (P6) and the dorsal pedicle of segment 5 (PPa) were exposed. **D** The PPa was transected and the anterior pedicle and P6 were isolated. **E–F** ICG-HSA was injected intravenously using an infusion pump for the first negative-staining procedure. Clear fluorescent demarcation was observed. **G**) The pedicle supplying dorsal segment 5 was dissected and occluded using a bulldog clamp. After that, IGC-HSA was injected a second time. **H** Fluorescent demarcation between segments 8 and 5 was observed. **I** An en-bloc specimen containing segments 5 and 6 was successfully resected. The middle hepatic vein and stump of G6/G5 were exposed on the resection surface

resection; moreover, it is associated with shorter operation time, lower intraoperative blood loss, lower complication rates, and better survival [16–18]. However, because of the low successful rate of existing fluorescent agents and the large differences in the dose and concentration of ICG reported by different centers [19, 20], the promotion and application of ICG fluorescence navigation technology in the real world are underutilized.

The success of ICG staining is mainly influenced by the following [21–24]: (1) clamping of the target Glissonean pedicle; (2) presence of extrahepatic arterial blood supply (e.g., accessory left hepatic artery, middle hepatic artery, and subphrenic artery); (3) presence of small branches in Glisson's capsule at the hepatic hilum; (4) gallbladder venous reflux; and (5) presence of communicating arterial and portal venous branches between the left and right hemilivers. In our study, patients without a clear ischemic line after intraoperative occlusion or separation of the target hepatic pedicle, and those with hepatic fluorescence reaching an intensity that interfered with the operation before intraoperative intravenous injection of ICG were excluded. The purpose of doing so was to minimize the influence of technique and anatomy on ICG fluorescence imaging so we could more accurately explore the feasibility of using the ICG-HSA complex in intraoperative NIF imaging.

Under normal conditions, ICG is non-fluorescent. However, when excited by near-infrared light, it undergoes fluorescence emission and can be used for fluorescence imaging [25]. Metabolism of ICG is divided into three stages: intravascular, liver, and systemic clearance [26]. After

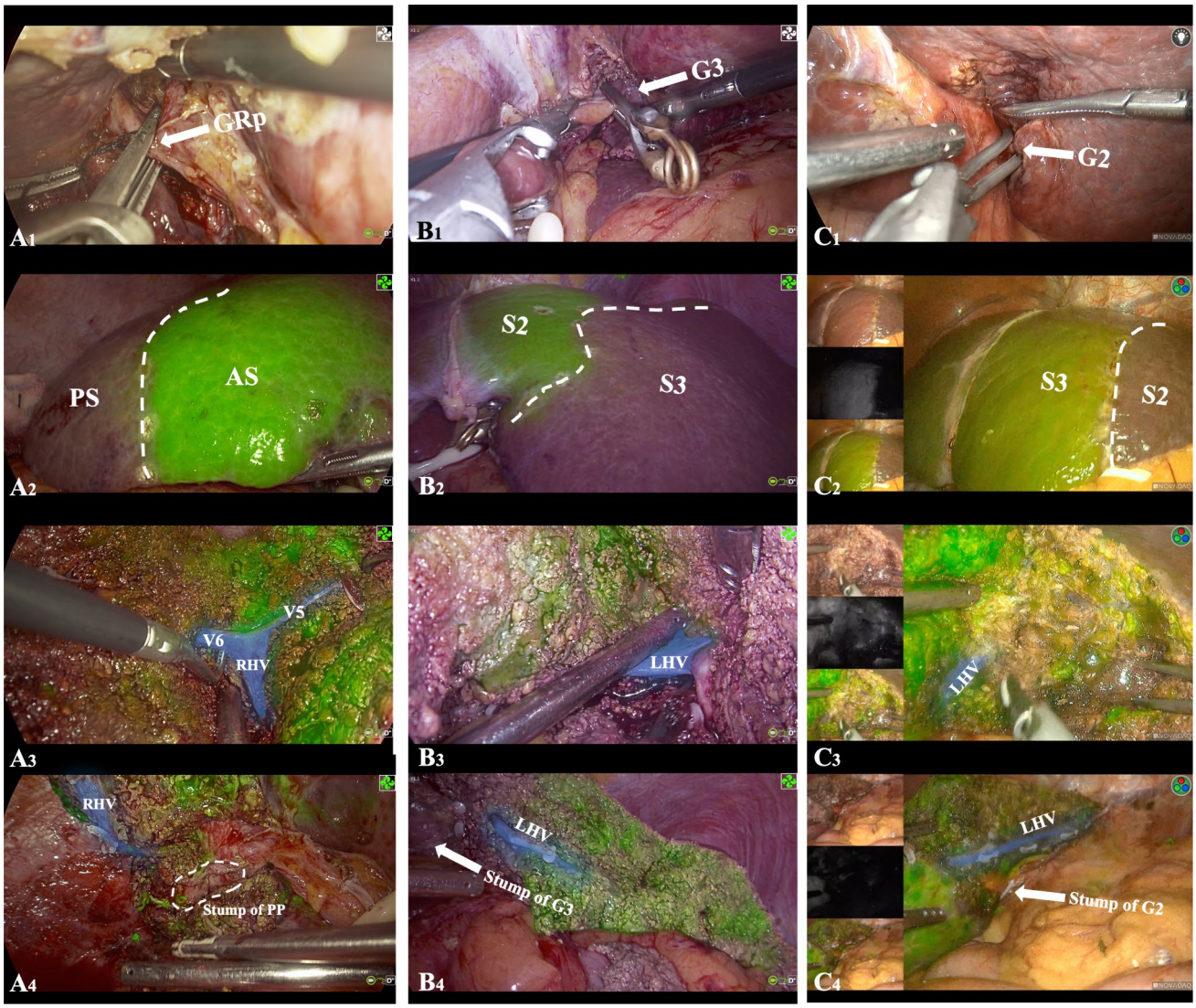

Fig. 4 **A** Laparoscopic right posterior segmentectomy: the extrahepatic Glissonean pedicle of the right posterior section (GRp) was clamped using a bulldog clamp (**A1**). After intravenous injection of ICG-HSA, clear fluorescent demarcation was observed between the posterior section (PS) and anterior section (AS) (**A2**). The landmark hepatic veins (V5, V6, and the right hepatic vein [RHV[) between the PS and AS were precisely located on the demarcation line (**A3**). After completion of the surgery, the entire course of the stump of the Posterior Pedicel (PP) and the RHV were visible (**A4**). **B & C** Laparoscopic hepatectomy of segments 2/3: the extrahepatic Glissonean pedicle of segments 2/3 (G3/G2) was clamped using a bulldog clamp (**B1/C1**). After intravenous injection of ICG-HSA, clear fluorescent demarcation was observed between S2 and S3 (**B2/C2**). The left hepatic vein (LHV) between S2 and S3 was precisely located on the demarcation line (**B3/C3**). After completion of the surgery, the entire course of the stump of G3/G2 and the LHV were visible (**B4/C4**)

intravenous injection, ICG enters the intravascular stage, where it mainly binds to plasma albumin and lipoproteins via non-covalent bonds with a binding rate of up to 98%. Albumin is the main carrier, which forms a relatively stable complex with ICG. Formation of albumin-ICG complexes does not change the basic structure of either molecule. The complexes are non-toxic and they reduce dye extravasation while increasing ICG stability. The tendency of plasma macromolecules to aggregate with ICG in the blood is a competitive process and in a dynamic equilibrium. Bound ICG is restricted and retained in blood vessels, with minimal leakage from the choriocapillaris, and is continuously brought to the liver through the circulation and specifically taken up by the liver [27]. Albumin, as a carrier of ICG, enters the hepatic sinusoids and is rapidly and efficiently taken up by hepatocytes, which begins the liver stage of ICG metabolism. ICG is transported into hepatocytes by the transporter proteins OATP1B3 and NTCP and then transported into the bile by glutathione s-transferase [27, 28]. However, the amount of plasma protein in blood vessels is limited. The non-conjugated binding form will become saturated as the number of ICG molecules increases. This causes

the injected ICG complex to release free ICG molecules, which are unstable. Without undergoing specific uptake by hepatocytes, the free molecules may reflux into the liver parenchyma through the hepatic venous system and directly leak out when the blood supply is unblocked. This can result in ectopic staining. Theoretically, the ICG-HAS complex should prevent the binding of ICG with other macromolecules and reduce free ICG, both of which cause ectopic staining. The complex should also reduce the destruction of the unstable double bond structure of ICG molecules by free oxygen, free sulfur, and other substances immediately after entering the circulation, thus preventing its inactivation and maintaining its fluorescence.

Our in vitro experimental results revealed that the ICG-HSA complex has superior optical properties and stability compared with free ICG, which is consistent with previous studies. Li et al. [10] reported that HSA can enhance the fluorescence quantum yield of ICG and improve its water solubility and photostability. Desmettre et al. [6] confirmed that HSA encapsulation can slow down the degradation and clearance of ICG and prolong its circulation time. In our study, the ICG-HSA complex demonstrated good stability under different temperature and time conditions, laying the foundation for its clinical application. However, previous studies have drawn different conclusions regarding the optimal binding ratio of HSA to ICG [7, 10]. The ratio we used requires further research and optimization.

ICG mainly relies on positive- or negative-staining techniques to achieve intraoperative fluorescence visualization and navigation of liver segments or lobes [29]. Successful ICG fluorescence staining can not only display the boundaries of liver segments or lobes on the liver surface but also clearly show the intersegmental plane in the deep liver parenchyma, especially in areas without hepatic veins. The positive staining method involves directly puncturing the target portal vein and injecting an appropriate amount of ICG to display the corresponding portal vein territory. This method requires advanced skill and is difficult to perform. In contrast, the negative-staining method involves occluding the target hepatic pedicle and then injecting ICG through a peripheral vein. By combining the traditional Glissonean pedicle approach with peripheral venous administration, the negative-staining method has a shorter learning curve. To achieve better clinical applicability and imaging success rates, we only used the negative-staining method in this study. Although the hepatic pedicles of all liver segments can be occluded via the extrahepatic approach [30], we did not include cases with tumors located in segment VII owing to technical limitations. The lesions in our study were successfully located in the fluorescence counterstaining area, which enabled us to achieve precise resection of the liver segments harboring the tumors. Our perioperative data (e.g., tumor margin distance, operation time, and intraoperative blood loss) were similar to those reported by Felli et al. [31] and a 2023 meta-analysis [32]. This indirectly reflects the feasibility of the technique. Furthermore, the stepwise fluorescence counterstaining technique with the ICG-HSA complex was successfully used to achieve precise combined liver segment resection of S5 and S6. With this surgical approach, the second-stage staining was possible because the first fluorescence staining showed almost no fluorescence drift. We believe that this further expands the scope of applicable surgical procedures for ICG-HSA fluorescence laparoscopic anatomical liver resection.

The safety of the ICG-HSA complex still needs further evaluation and discussion. Although none of our patients experienced a significant adverse event, and their residual liver function recovered well after surgery, studies comprising a larger number of patients are needed. Nonetheless, both ICG and HSA are approved by the United States Food and Drug Administration and are widely recognized for their safety. However, when the two are combined, theoretically, HSA can slow down the clearance of ICG and prolong its retention time in the liver, which is conducive to continuous and stable fluorescence imaging during surgery. It is unclear whether a delay in ICG metabolism and excretion will increase the risk of drug accumulation toxicity [6, 33]. In the future, it will be necessary to conduct dedicated in vivo pharmacokinetic and safety evaluation trials of the ICG-HSA complex and examine any associated long-term changes in liver and kidney function.

This study has several limitations. First, the sample size was relatively small and there was no control group. Large-scale prospective randomized controlled trials will be needed to evaluate the clinical efficacy of the ICG-HSA complex. Second, most study patients had good liver function; therefore, the value of the ICG-HSA complex in patients with liver dysfunction is still unclear. Ishizawa et al. [29] suggested that the clearance rate of ICG is significantly lower in patients with cirrhosis, which reduces the quality of fluorescence imaging. They recommended that patients with liver cirrhosis should receive higher doses of ICG or undergo longer waiting times to obtain satisfactory imaging. Whether the ICG-HSA complex can overcome this traditional limitation is worthy of further investigation.

Conclusion

ICG-HSA complex-mediated fluorescence-assisted laparoscopic anatomical liver resection is safe and feasible. Compared with free ICG, the novel ICG-HSA complex has better optical properties and in vivo stability, which can improve the accuracy of intraoperative liver segment localization and optimize the anatomical plane. Based on this, the stepwise negative-staining technique can achieve anatomical resection

of combined liver segments. We expect the ICG-HSA complex to become an ideal agent for fluorescence imaging in anatomical liver resection.

Supplementary Information The online version contains supplementary material available at https://doi.org/10.1007/s00464-024-11295-8.

Acknowledgements We thank all those who provided support and assistance for the study. We also thank Liwen Bianji (Edanz) (https://www.liwenbianji.cn) for editing the English text of a draft of this manuscript.

Funding This work was supported by grants from the National Natural Science Foundation of China (82173124, 82103533, 81972747, and 82203823), the Natural Science Foundation of Sichuan Province (2023NSFSC1877), and the Science and Technology Program of Sichuan Province (2023JDR0077, 2022YFQ0077).

Data accessibility The raw data supporting the conclusions of this manuscript will be made available by the corresponding author, without undue reservation, to any qualified researcher.

Declarations

Disclosures Drs. Fengwei Gao, Qingyun Xie, Xiaoyun Ran, Xin Zhao, Manyu Yang, Kangyi Jiang, Tianyang Mao, Jiayin Yang, Kun Li, and Hong Wu have no conflicts of interest or financial ties to disclose.

Ethical approval The study protocol for the use of ICG-HSA complexes and the prospective clinical trial was reviewed and approved by the Clinical Research Ethics Committee of West China Hospital, Sichuan University (approval number: 2023 review (2121)). The study was registered on ClinicalTrials.gov (registration number: NCT06219096). All participants voluntarily agreed to take part in the study and provided written informed consent prior to enrollment. The study was conducted in compliance with the Declaration of Helsinki and all relevant guidelines and regulations for research involving human subjects, human material, or human data. The authors confirm that informed consent was obtained from all study participants.

Patient consent statement The authors confirmed that informed consent was obtained from all subjects.

References

1. Sung H, Ferlay J, Siegel RL et al (2021) Global cancer statistics 2020: GLOBOCAN estimates of incidence and mortality worldwide for 36 cancers in 185 countries. CA Cancer J Clin 71(3):209–249. https://doi.org/10.3322/caac.21660
2. Jiao S, Li G, Zhang D, Xu Y, Liu J, Li G (2020) Anatomic versus non-anatomic resection for hepatocellular carcinoma, do we have an answer? A meta-analysis Int J Surg 80:243–255. https://doi.org/10.1016/j.ijsu.2020.05.008
3. Liao K, Yang K, Cao L et al (2022) Laparoscopic anatomical versus non-anatomical hepatectomy in the treatment of hepatocellular carcinoma: a randomised controlled trial. Int J Surg 102:106652. https://doi.org/10.1016/j.ijsu.2022.106652
4. Terasawa M, Ishizawa T, Mise Y et al (2017) Applications of fusion-fluorescence imaging using indocyanine green in laparoscopic hepatectomy. Surg Endosc 31(12):5111–5118. https://doi.org/10.1007/s00464-017-5576-z
5. Wang X, Teh CSC, Ishizawa T et al (2021) Consensus guidelines for the use of fluorescence imaging in hepatobiliary surgery. Ann Surg 274(1):97–106. https://doi.org/10.1097/SLA.0000000000004718
6. Desmettre T, Devoisselle JM, Mordon S (2000) Fluorescence properties and metabolic features of indocyanine green (ICG) as related to angiography. Surv Ophthalmol 45(1):15–27. https://doi.org/10.1016/S0039-6257(00)00123-5
7. Zheng C, Zheng M, Gong P et al (2012) Indocyanine green-loaded biodegradable tumor targeting nanoprobes for in vitro and in vivo imaging. Biomaterials 33(22):5603–5609. https://doi.org/10.1016/j.biomaterials.2012.04.044
8. Saxena V, Sadoqi M, Shao J (2003) Degradation kinetics of indocyanine green in aqueous solution. J Pharm Sci 92(10):2090–2097. https://doi.org/10.1002/jps.10470
9. Jiang JX, Keating JJ, Jesus EMD et al (2015) Optimization of the enhanced permeability and retention effect for near-infrared imaging of solid tumors with indocyanine green. Am J Nucl Med Mol Imaging 5(4):390–400
10. Li Y, Dai C, Hua Z et al (2024) A human serum albumin-indocyanine green complex offers improved tumor identification in fluorescence-guided surgery. Trans Cancer Res. https://doi.org/10.21037/tcr-23-2338
11. Agha RA, Sohrabi C, Mathew G et al (2020) The PROCESS 2020 guideline: updating consensus preferred reporting of case series in surgery (PROCESS) guidelines. Int J Surg 84:231–235. https://doi.org/10.1016/j.ijsu.2020.11.005
12. Clavien PA, Barkun J, de Oliveira ML et al (2009) The Clavien-Dindo classification of surgical complications: five-year experience. Ann Surg 250(2):187–196. https://doi.org/10.1097/SLA.0b013e3181b13ca2
13. Fanali G, di Masi A, Trezza V, Marino M, Fasano M, Ascenzi P (2012) Human serum albumin: from bench to bedside. Mol Aspects Med 33(3):209–290. https://doi.org/10.1016/j.mam.2011.12.002
14. Gotohda N, Cherqui D, Geller DA et al (2022) Expert consensus guidelines: how to safely perform minimally invasive anatomic liver resection. J Hepatobiliary Pancreat Sci 29(1):16–32. https://doi.org/10.1002/jhbp.1079
15. Cho JY, Han HS, Wakabayashi G et al (2018) Practical guidelines for performing laparoscopic liver resection based on the second international laparoscopic liver consensus conference. Surg Oncol 27(1):A5–A9. https://doi.org/10.1016/j.suronc.2017.12.003
16. Chen H, Wang Y, Xie Z et al (2022) Application effect of ICG fluorescence real-time imaging technology in laparoscopic hepatectomy. Front Oncol 12:819960. https://doi.org/10.3389/fonc.2022.819960

17. Liu F, Wang H, Ma W et al (2023) Short- and long-term outcomes of indocyanine green fluorescence navigation- versus conventional-laparoscopic hepatectomy for hepatocellular carcinoma: a propensity score-matched, retrospective. Cohort Study Ann Surg Oncol 30(4):1991–2002. https://doi.org/10.1245/s10434-022-13027-5
18. Itoh S, Tomiyama T, Morinaga A et al (2022) Clinical effects of the use of the indocyanine green fluorescence imaging technique in laparoscopic partial liver resection. Ann Gastroenterol Surg 6(5):688–694. https://doi.org/10.1002/ags3.12563
19. Xu Y, Chen M, Meng X et al (2020) Laparoscopic anatomical liver resection guided by real-time indocyanine green fluorescence imaging: experience and lessons learned from the initial series in a single center. Surg Endosc 34(10):4683–4691. https://doi.org/10.1007/s00464-020-07691-5
20. Wakabayashi T, Cacciaguerra AB, Abe Y et al (2022) Indocyanine green fluorescence navigation in liver surgery: a systematic review on dose and timing of administration. Ann Surg 275(6):1025–1034. https://doi.org/10.1097/SLA.0000000000005406
21. Sugita M, Ryu M, Satake M et al (2000) Intrahepatic inflow areas of the drainage vein of the gallbladder: analysis by angio-CT. Surgery 128(3):417–421. https://doi.org/10.1067/msy.2000.107380
22. Kai K, Satoh S, Watanabe T, Endo Y (2010) Evaluation of cholecystic venous flow using indocyanine green fluorescence angiography. J Hepatobiliary Pancreat Sci 17(2):147–151. https://doi.org/10.1007/s00534-009-0111-9
23. Tohma T, Cho A, Okazumi S et al (2005) Communicating arcade between the right and left hepatic arteries: evaluation with CT and angiography during temporary balloon occlusion of the right or left hepatic artery. Radiology 237(1):361–365. https://doi.org/10.1148/radiol.2371040919
24. van Lienden KP, Hoekstra LT, Bennink RJ, van Gulik TM (2013) Intrahepatic left to right portoportal venous collateral vascular formation in patients undergoing right portal vein ligation. Cardiovasc Intervent Radiol 36(6):1572–1579. https://doi.org/10.1007/s00270-013-0591-5
25. Landsman ML, Kwant G, Mook GA, Zijlstra WG (1976) Light-absorbing properties, stability, and spectral stabilization of indocyanine green. J Appl Physiol 40(4):575–583. https://doi.org/10.1152/jappl.1976.40.4.575
26. Levesque E, Martin E, Dudau D, Lim C, Dhonneur G, Azoulay D (2016) Current use and perspective of indocyanine green clearance in liver diseases. Anaesth Crit Care Pain Med 35(1):49–57. https://doi.org/10.1016/j.accpm.2015.06.006
27. de Graaf W, Häusler S, Heger M et al (2011) Transporters involved in the hepatic uptake of (99m)Tc-mebrofenin and indocyanine green. J Hepatol 54(4):738–745. https://doi.org/10.1016/j.jhep.2010.07.047
28. Cui Y, König J, Leier I, Buchholz U, Keppler D (2001) Hepatic uptake of bilirubin and its conjugates by the human organic anion transporter SLC21A6. J Biol Chem 276(13):9626–9630. https://doi.org/10.1074/jbc.M004968200
29. Ishizawa T, Zuker NB, Kokudo N, Gayet B (2012) Positive and negative staining of hepatic segments by use of fluorescent imaging techniques during laparoscopic hepatectomy. Arch Surg 147(4):393–394. https://doi.org/10.1001/archsurg.2012.59
30. Berardi G, Igarashi K, Li CJ et al (2021) Parenchymal sparing anatomical liver resections with full laparoscopic approach: description of technique and short-term results. Ann Surg 273(4):785–791. https://doi.org/10.1097/SLA.0000000000003575
31. Felli E, Ishizawa T, Cherkaoui Z et al (2021) Laparoscopic anatomical liver resection for malignancies using positive or negative staining technique with intraoperative indocyanine green-fluorescence imaging. HPB 23(11):1647–1655. https://doi.org/10.1016/j.hpb.2021.05.006
32. Zhou K, Zhou S, Du L et al (2023) Safety and effectiveness of indocyanine green fluorescence imaging-guided laparoscopic hepatectomy for hepatic tumor: a systematic review and meta-analysis. Front Oncol 13:1309593. https://doi.org/10.3389/fonc.2023.1309593
33. Porcu EP, Salis A, Gavini E, Rassu G, Maestri M, Giunchedi P (2016) Indocyanine green delivery systems for tumour detection and treatments. Biotechnol Adv 34(5):768–789. https://doi.org/10.1016/j.biotechadv.2016.04.001